DEXTEROUS EXTERNAL SPACE MANIPULATION: SERIAL OR PARALLEL CONCEPTS COMPARISON

D. Alazard — J.P. ChrétienCERT-ONERA/DERA

2, Avenue E. Belin

TOULOUSE

France

Tel. (33) 61.55.70.15. — Fax. (33) 61.55.71.94

e-mail alazard@saturne.cert.fr

Paper presented at IFAC
Aotomatic Control in Aerospace 94
Palo Alto (CA)
Sept. 12th-16th, 1994

DEXTEROUS EXTERNAL SPACE MANIPULATION: SERIAL OR PARALLEL CONCEPTS COMPARISON

D. Alazard — J.P. Chrétien

CERT/DERA
2, Avenue E. Belin
TOULOUSE
France

Abstract: *Within the external space manipulation framework, we compare two concepts to achieve an accurate positioning of the manipulator end effector. The first one involves a serial mini-manipulator inserted between the external space manipulator (macro-manipulator) and the end effector. Then, an anchorage mechanism is required to provide a hold point to the macro / mini manipulators interface. This solution can be called: static positioning of the mini-manipulator base. The anchorage system stiffness is then discussed. In the second concept, the mini-manipulator serial architecture is replaced by a light parallel architecture. The macro manipulator is then used to provide a dynamic positioning to the mini-manipulator base by the mean of a coordinated control scheme between both manipulators.*

Keywords: SPACE MANIPULATORS — SERIAL ARCHITECTURE — PARALLEL ARCHITECTURE — FLEXIBLE MODES — COORDINATED CONTROL — DEXTEROUS MANIPULATION

Introduction

The dynamic Cartesian positioning accuracy of a manipulator controlled from proximity information depends upon the artificial stiffness (created by the control law) between its base and its end effector. This stiffness is directly given, via the Jacobian transformation, by the proportional gains of joint position servo-loops i.e. the closed loop joint dynamic. In the case of an external space manipulator joints like ERA or RMS, we have shown in a previous paper [1] that this dynamic is limited by the joint cantilevered pulsation which is always very low because the inertia seen from the joint is very large (by the fact of very long beams) and the in-joint compliance is low (the 0g environment and the weight constraints yield to a very light motorization with a too flexible gear-box). Then, such a manipulator can generate a very large work-space but does not allow to point its end effector with a precision under 1 centimeter (Fig 6). Static positioning errors can be improved by control tricks such as integral terms, friction feedforward compensations or gains w.r.t configuration updating. But these artifices do not permit to obtain the dynamic performance required to drive back dynamic perturbations (for instance: carrier vehicle motion, dry friction or motor harmonic disturbance) at the time of path tracking tasks. For these tasks or for manipulating small objects, a dexterous manipulator (or mini-manipulator) inserted between this macro-manipulator and its end effector is needed to get a sharp pointing (precision under 1 millimeter).

This work has been performed under contracts granted by C.N.E.S. — Centre Spatial de Toulouse (France) under the technical management of M. Maurette

To reach a such precision, two solutions can be investigated:

- a stabilization device (or anchorage system) linking the macro and mini manipulators interface to a massive body (the chaser, the target or any other massive spacecraft) may be used to immobilize the last body of the macro-manipulator and to provide an hold point to the base of the mini-manipulator. We will call this solution: *static positioning* of the dexterous manipulator. The stabilization device will have only a few distant space distributed anchorage points. So, the mini-manipulator must have an adequate reachable area (typically: 2 meters): the best mechanical design is then a serial arm involving non-negligible inertias and so non-negligible macro/mini manipulators dynamic coupling terms. These terms do not enable a coordinate control of both manipulators as will be proposed in the second solution. It will be also shown that the carrier arm with all its joints braked can not provide a stable base by the fact of the in-joint and beam distributed flexiblities and so justify the anchorage device. Then the problem is to specify, according to the mechanical characteristics of both manipulators, the stiffness and the damping of this anchorage device allowing end effector motions with the required speed and accuracy. (see Fig 7)
- the dexterous manipulator have a sufficient dynamic to guarantee the required end effector positioning accuracy in the presence of residual motions of its base and disturbances caused by the dynamic coupling between the dexterous and the carrier manipulator. To minimize these disturbances, the mini-manipulator must be light and fast and so, the best mechanical

design is a parallel arm. The working space of a such manipulator is too small, so this solution will use the macro manipulator to carry out a *dynamic positioning* of the dexterous manipulator base by the mean of a coordinated control sharing the motion between the low dynamic component (controlled by the macro manipulator) and the high dynamic component (controlled by the dexterous manipulator). The feasibility of a such control from the only proximity information must be proved and an evaluation of the servo-loop bandwidths of both manipulators is needed. (see Fig 8)

This paper is divided in three sections. The first one summarizes the various assumptions under which the comparison will be done. The dynamic performances of the macro manipulator equipped with a proximeter are presented to justify the need of a dexterous manipulator.

The second and the third section will be devoted to the serial and the parallel concepts respectively. Modeling, control and simulation considerations are proposed for both solution.

1 Generalities

1.1 Simulation assumptions

For each concept, several dynamic perturbations have been taken into account:

- carrier vehicle motion (accelerations due to its own AOCS)
- in-joint dry ant viscous friction
- proximity measurement noise
- joint position encoder and tachometer quantizations

The most determinant perturbation ([2]) is the in-joint dry friction which obliges us to drive hard the control gains. So, the most representative criterium to decide between the different concepts is the greatest Cartesian position servo-loop bandwidth.

In order to simplify the various analysis which will follow, we will assume, here, that the carrier vehicle is fixed.

The prescribed reference motion on which the solutions will be validated is composed of two successive and opposite position ramps and can represents the residual motion of a target which is roughly stabilized (see fig 10). On a $10s$ horizon the motion magnitude is $30cm$ along X axis (in the manipulator plane) and $5cm$ along Y axis (transverse axis; see figure 6 for axis orientation).

1.2 Macro manipulator dynamic

The macro manipulator geometric skeleton is roughly displayed on figure 6. The joint configuration (from the shoulder to the end effector) chosen to compare the different solutions reads:

$$[0 \quad 135^o \quad 90^o \quad -45^o \quad 0 \quad 0]$$

and corresponds to a middle planar configuration without any kinematic similarities.

The total arm length is $6.5m$ and the various joints, in the middle configuration, bear the inertias I_c given in the table 1 with the corresponding stiffness K_j, rotor inertias I_r and cantilevered ω_e and free ω_l pulsations.

joint	I_c Kgm^2	K_j Nm/rd	I_r Kgm^2	ω_e rd/s	ω_l rd/s
1	1000.	200000	33.75	14.	78.
2	1000.	200000	33.75	14.	78.
3	550.	200000	18.	19.	107.
4	30.	200000	3.75	81.	250.
5	15.	200000	3.75	115.	260.
6	4.	rigid	3.75	/	/

Table 1 Joint dynamic parameters of macro manipulator

We can notice (mainly for the both shoulder joints and the elbow joint) a very low cantilevered w.r.t free pulsation ratios. In [1], we have shown that this pulsation ratio is the joint basic parameter which determines the greatest joint bandwidth achievable with the classical proportionnal-derivative control. This limit is also reduced by dynamic couplings between the six joints which spread out the closed loop eigenvalues on the real axis and so can destabilize the system at the time of the sampling. Furthermore, an isotropic Cartesian behavior yields to tune each joint with the same dynamic ([2]). Considering a $200Hz$ sample rate, the best closed loop dynamic have been obtained with a local P.D. control tuned over damped at $\omega = 4rd/s$. From the proximity information δX and joint rate measurements $\dot{Q}$, the macro manipulator control requires the inverse Jacobian transformation and reads:

$$U = diag(I_c)\left[\omega^2.J^{-1}\delta X - 2.\omega.\dot{Q}\right] \qquad \omega = 4\ rd/s \tag{1}$$

The simulation of the macro manipulator controlled by such a control law is displayed on figure 10 and reveals important tracking errors (over 1 cm in any direction) and so justifies a dexterous manipulator to reach the required accuracy.

2 Serial concept

2.1 Dynamic model

A rough sketch of the set composed of the macro manipulator, the mini manipulator and the anchorage system is displayed on figure 7. The geo-dynamic skeleton of the mini manipulator is modeled on the macro manipulator with a smaller scale. Its deployed length is $1.75m$ and the joint configuration is symmetrical to the macro manipulator one, let (from the shoulder to the end effector):

$$[0 \quad 45^o \quad 90^o \quad -45^o \quad 0 \quad 0]$$

Each joint has a $50Nm$ available drive torque and bears the following inertias:

$$[30. \quad 25. \quad 15. \quad 3.3 \quad 1.8 \quad 0.5]_{Nm}$$

These dynamic parameters enable us to appreciate the great acceleration ability of this arm and if we consider

it on a fixed base, there are not any difficulties, from classical P.D. network like the previous one, to drive hard the control gains until the required closed loop performances are reached. So, the control of the mini manipulator will not interest us any longer. We will adopt the same law as the macro manipulator i.e (equation (1)): each joint is tuned over damped at the same frequency ω on its current inertia; goods results have been obtained with $\omega = 15rd/s$. We prefer to highlight here the dynamic parameters, in terms of stiffness and damping of the anchorage device.

Some extra assumptions have to be added here: the inner anchorage point connected to the space station in figure 7 will be supposed immobile like the carrier vehicle. Furthermore and as a consequence of mass constraints within the space framework, the anchorage device must be light w.r.t to the manipulators, so its mass will be neglected. From the simulation point of view, this assumption enables us to use multi-body dynamic software dedicated to flexible open chain. For this application, we have used SMASP software (Simulation d'un bras MAnipulateur SPatial [3]) which allows to take into account the in-joint flexibilities, efficient in-joint dry friction models and to apply external forces on any point of any body. From the 12 d.o.f chain representing the set of both manipulators, this last facility is used to simulated the anchorage system by computing the reaction wrench F applied by the anchorage device on the macro manipulator last body (i.e. the mini manipulator base):

$$F = -K_a.\delta X_a - D_a\delta\dot{X}_a$$

where K_a, D_a design respectively the anchorage stiffness and damping at the connecting point between the three subsets and δX_a the displacement of this point w.r.t to the anchorage base (all these variables must be expressed in the same frame).

Then, the linear open loop joint dynamic model of the mini manipulator mounted on the flexible structure, composed of the macro manipulator in braking mode and in parallel with the anchorage system, reads:

$$\begin{bmatrix} A_{pp} & A_{pr} \\ A_{rp} & A_{rr} \end{bmatrix} \begin{bmatrix} \ddot{Q}_p \\ \ddot{Q}_r \end{bmatrix} + \begin{bmatrix} D_{pp} + {J_p^a}^T D_a J_p^a & \phi \\ \phi & \phi \end{bmatrix} \begin{bmatrix} \dot{Q}_p \\ \dot{Q}_r \end{bmatrix} + \begin{bmatrix} K_{pp} + {J_p^a}^T K_a J_p^a & \phi \\ \phi & \phi \end{bmatrix} \begin{bmatrix} Q_p \\ Q_r \end{bmatrix} = \begin{bmatrix} \phi \\ 1_{6\times 6} \end{bmatrix} U \quad (2)$$

The proximity measurement and the control law reads:

$$\begin{aligned} &\delta X = X_{ref} - [J_p^e \quad J_r^e] \begin{bmatrix} Q_p \\ Q_r \end{bmatrix}; \\ &U = K_p (J_r^e)^{-1} \delta X - K_v Q_r; \text{ with} \\ &K_p = \omega^2.diag(A_{rr});\ K_v = 2.\omega.diag(A_{rr}) \end{aligned} \quad (3)$$

where:

- Q_p macro manipulator joint d.o.f vector
- Q_r mini manipulator joint d.o.f vector
- U mini manipulator joint torque vector
- K_{pp} macro manipulator joint stiffness matrix
- D_{pp} macro manipulator joint damping matrix (negligible)
- J_p^a macro manipulator Jacobian (at the anchorage point)
- J_p^e macro manipulator Jacobian (at the end effector)
- J_r^e mini manipulator Jacobian (at the end effector)
- $\begin{bmatrix} A_{pp} & A_{pr} \\ A_{rp} & A_{rr} \end{bmatrix}$ total joint mass matrix

It can be easily shown that the nominal control tuning ($\omega = 15rd/s$) becomes unstable when the stiffness alone of the macro manipulator (without anchorage system) is used. This unstable behavior is the result of the non-collocation between the mini manipulator actuator and the absolute position measurement (w.r.t the inertial frame) provided by the proximeter and can be better apprehended on the following equivalent mono-dimensional case:

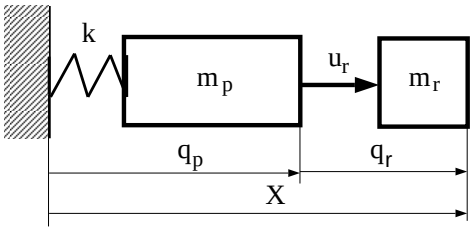

Figure 1 Equivalent mono-dimentional model

where indexes p and r are relative respectively to the macro and mini manipulator parameters. If we neglect the dissipative terms, the open loop model is then reduced to:

$$\begin{bmatrix} m_p + m_r & m_r \\ m_r & m_r \end{bmatrix} \begin{bmatrix} \ddot{q_p} \\ \ddot{q_r} \end{bmatrix} + \begin{bmatrix} k & 0 \\ 0 & 0 \end{bmatrix} \begin{bmatrix} q_p \\ q_r \end{bmatrix} = \begin{bmatrix} 0 \\ u \end{bmatrix}$$

This equation is characterized by two dynamic parameters:

- the free pulsation:$\omega_l = \sqrt{\frac{k}{m_p}}$
- the cantilevered pulsation:$\omega_e = \sqrt{\frac{k}{m_p + m_r}}$

We have shown in [2] that the control law:

$$u = m_r\omega^2(X_{ref} - X) - 2m_r\omega\dot{q_r}\ ,$$

is stable as long as the tuning verifies:

$$\omega < \omega_e \text{ or } K_p = m_r\omega^2 < \frac{k}{1 + m_p/m_r} \quad (4)$$

This condition shows how the anchorage stiffness and the both manipulator mass ratio limit the closed-loop bandwidth.

2.2 Anchorage stiffness and damping analysis

In the multi-dimensional case which interest us, the stability condition (4) depends strongly upon the three subset configurations and can not be simply expressed. In order to reduce the parametric variations, we have considered an anchorage devise working only along the three translations with an isotropic behavior, let (in

the nominal X, Y, Z frame attached to the anchorage point):

$$K_a = diag([k \quad k \quad k \quad 0 \quad 0 \quad 0])$$
$$D_a = diag([d \quad d \quad d \quad 0 \quad 0 \quad 0])$$

The multi-variable roots locus displayed on figure 2 and 3 represent the evolution of the closed-loop low frequencies dynamic (from equations (2) and (3)) with respect respectively to the reduced anchorage stiffness ($0 < k < 10000\ N/m\ ; d = 0.$) and the reduced damping anchorage ($0 < d < 1000\ Ns/m\ ; k = 0.$).

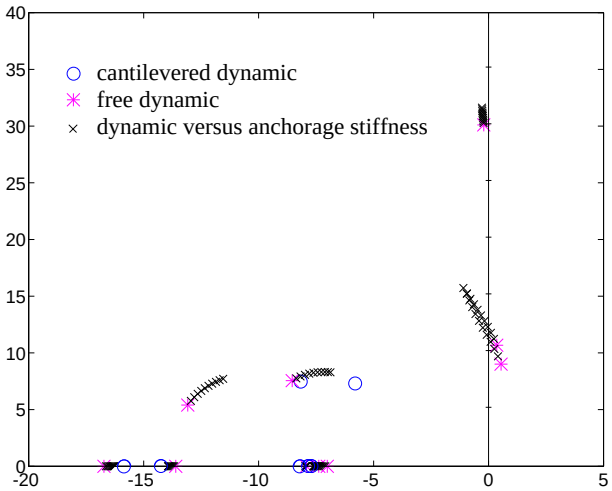

Figure 2 Dynamic evolution w.r.t anchorage stiffness

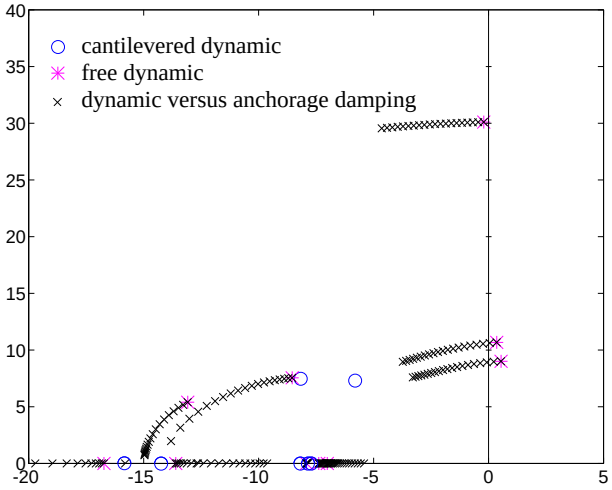

Figure 3 Dynamic evolution w.r.t anchorage damping

On both plots, we can note the macro manipulator joint flexible modes coupled with the mini manipulator rigid modes. The two lowest flexible mode are unstable for $k = 0.$ and $d = 0.$. For higher values of the stiffness k (Fig 2), flexible modes are driven far on the imaginary axis while rigid modes are attracted to the ideal cantilevered closed-loop dynamic (obtained with a fixed base). This cantilevered dynamic represents the transmission zeros of the multivariable transfer between the force wrench and the position at the anchorage point. The same remarks can be done on figure 3 but flexible mode are now driven far on the stable real axis.

If we consider the residues of the first flexible modes, seen from the end effector position, we can notice ([2]) that they can be soon reduced as the anchorage stiffness increases: for the value we have chosen ($k = 10000N/m$) flexible modes are quasi unobservable from end effector position. Higher values should certainly give better results but should not be compatible with a negligible mass anchorage system.

The anchorage damping is naturally more efficient to stabilize the closed loop system, but an adequate value like $d = 1000Ns/m$ is not realist and can not be reached with the natural damping of the material which are liable to be used for the anchorage device in the space environment framework. An alternative consists in creating artificial damping from the macro manipulator joint whose stiffness are redundant with the anchorage system ones. So, the solution we have finally adopted uses the anchorage system (with $k = 10000N/m$ and $d = 0Ns/m$) to hold the mini-manipulator base along translational d.o.f, the three wrist joint of the macro-manipulator in braking mode to hold this base along rotational d.o.f while the two shoulder joints and elbow joint of the macro-manipulator are servo-looped on their current positions. The global stiffness is then reduced because position servo-loop proportional gains are lower than the corresponding joint stiffness, but the artificial damping created by the derivative terms enable to increase the global closed-loop dynamic.

2.3 Simulation results

The time response of the end effector along the nominal motion is displayed on figure 10 and reveals significant improvement w.r.t the solution obtained with the macro-manipulator alone. Only the tracking errors along the Z axis derived from in-joint dry friction is above the specifications.

3 Parallel concept

Figure 9 shows a rough sketch of the parallel dexterous manipulator (from CNES data).

Geometric, kinematic and dynamic models of such a Stewart like platform are heavy to be presented here and have already been the subject of several papers [4]. Analytical models which takes explicitly into account the joint constraints have been established and are detailed in [5]. These results have been validated with a multi-body dynamic software called SDFAST which is a powerful tool for mechanism with kinematic loops considering the complexity of this problem: 20 bodies (2 plates, 6 rotors, 6 pistons and 6 cylinders) , 30 d.o.f for the open chain and 18 joints constraints. We just want to highlight some specific features of this particular parallel structure from the kinematic and dynamic behaviors point of view and which will be determinant for the control design.

3.1 Kinematic model

For parallel structure, the inverse kinematic model can be expressed more easily than direct model which requires therefore one matrix inversion. In the middle configuration, the inverse Jacobian matrix $J_0^{-1}$of point B (the end effector center) w.r.t the lower plate written in the frame A reads:

$$\begin{pmatrix} 0.986 & 0 & 0.168 & -0.005 & -0.038 & 0.032 \\ 0.986 & 0 & 0.168 & 0.005 & -0.038 & -0.032 \\ 0.986 & -0.146 & -0.084 & -0.005 & -0.008 & -0.049 \\ 0.986 & -0.146 & -0.084 & 0.005 & 0.046 & -0.017 \\ 0.986 & 0.146 & -0.084 & -0.005 & 0.046 & 0.017 \\ 0.986 & 0.146 & -0.084 & 0.005 & -0.008 & 0.049 \end{pmatrix}$$

Note: The joint coordinates are the jack length variations (m) and upper plate linear and angular velocities are expressed in m/s and rd/s respectively.

We can notice the low values of fourth colon. If we consider now the elementary jack stiffness k along its axis (i.e. the proportional gain of its position servo-loop or the real jack stiffness if it is locked), the global Cartesian stiffness seen from the end effector reads:

$$K_{cart} = k.J^{-T}J = 10^3. \begin{pmatrix} 10\,495 & 0 & 0 & 0 & 0 & 0 \\ 0 & 153 & 0 & 0 & 0 & 34 \\ 0 & 0 & 153 & 0 & -34 & 0 \\ 0 & 0 & 0 & 0.3 & 0 & 0 \\ 0 & 0 & -34 & 0 & 13 & 0 \\ 0 & 34 & 0 & 0 & 0 & 13 \end{pmatrix}$$

and exhibits a very great stiffness along Ax axis (a six parallel jacks set) but a very low one around this axis. This parallel manipulator has not an isotropic kinematic behavior in Cartesian frame and is not suitable to control the motion around its symmetrical axis and so, that justifies the terminal rotation. In order to simplify the problem and considering that this d.o.f. does not have to work at the time of linear motions (which are the most demonstrative of space manipulations), we have not taken into account this terminal rotation.

3.2 Dynamic model

The main dynamic characteristic of this concept is the electric motorization because the great screw transmission ratio ($15079 rd/m$) leads to very important apparent masses of rotor inertias. Indeed, in middle configuration, the Cartesian dynamic model (mass matrix) M_0 at the end effector center (B) and projected in fixed frame A reads:

$$\begin{pmatrix} 2670 & 0 & 0 & 0 & 0 & 0 \\ 0 & 55.8 & 0 & 0 & 0 & 10.6 \\ 0 & 0 & 55.8 & 0 & 10.6 & 0 \\ 0 & 0 & 0 & 0.15 & 0 & 0 \\ 0 & 0 & 10.6 & 0 & 3.70 & 0 \\ 0 & 10.6 & 0 & 0 & 0 & 3.70 \end{pmatrix}$$

and reveals a 2.6 tons mass along Ax axis and therefore, a non-isotropic Cartesian dynamic behavior. Note that the acceleration ability does not suffer of such a mass because the driving force along this axis benefits also by this transmission ratio: each jack can apply a 850 N force along its axis. But in none symmetric (w.r.t to Ax axis) configuration cases, this rotors apparent mass reveals non negligible projections along transverse axis. Therefore, the Cartesian dynamic model is very variant w.r.t the configuration. If we consider now the joint dynamic model in the middle configuration A_0, which reads:

$$A_0 = J_0^T M_0 J_0 = \begin{pmatrix} 631 & -40.8 & 11.0 & -7.44 & 11.0 & -147 \\ -40.8 & 631 & -147 & 11.0 & -7.44 & 11.0 \\ 11.0 & -147 & 631 & -40.8 & 11.0 & -7.44 \\ -7.44 & 11.0 & -40.8 & 631 & -147 & 11.0 \\ 11.0 & -7.44 & 11.0 & -147 & 631 & -40.8 \\ -147 & 11.0 & -7.44 & 11.0 & -40.8 & 631 \end{pmatrix}$$

we can notice very great diagonal terms (rotor apparent mass in jack direction is equal to 450 Kg) which are maintained at the time of configuration changes.

3.3 Control design

From the control law synthesis point of view, these results are essentials: the linear open loop model without taking into account coriofugal terms or natural damping reads:

$$M(Q)\ddot{X} = J^{-T}(Q).U \quad or$$
$$A(Q)\ddot{Q} = U$$

Where X designs the Cartesian position six components vector; Q, the generalized joint coordinates vector and U the generalized joint forces vector (jack forces).

It seems natural to tune the control gain on middle dynamic model (real time gains updating with configuration requires mass matrix computation and can not be envisaged at the same sample rate as the control). Then there are two well-known control laws which can generate Cartesian uncoupled motions:

- a control based on middle Cartesian dynamic model which reads:

  $$U = J^T(Q)M_0\left[K_p(X_{ref} - X) + K_v\left(\dot{X}_{ref} - \dot{X}\right)\right]$$

  and which is often used for parallel architecture whose dynamic behavior is governed by end effector mass/inertias. The closed loop characteristic equation then reads:

  $$Ms^2 + M_0K_vs + M_0K_p = 0_{6\times6}$$

- a control based on middle joint dynamic model which reads:

  $$U = A_0J^{-1}(Q)\left[K_p(X_{ref} - X) + K_v\left(\dot{X}_{ref} - \dot{X}\right)\right]$$

  more often used for serial manipulator. The closed loop characteristic equation becomes:

  $$Ms^2 + J^{-T}A_0J^{-1}K_vs + J^{-T}A_0J^{-1}K_p = 0_{6\times6}$$

In both cases proportional and derivative gains (K_p and K_v) are tuned to get an isotropic Cartesian behavior ($K_p = \omega^2.I_{6\times6}$; $K_v = 2.\omega.I_{6\times6}$) and lead, in the middle configuration, to 12 eigenvalues equals to ω. But the evolution of this closed loop dynamic w.r.t the configuration are quite different:

- in the first case, there are some configurations for which dynamic couplings drive far on real axis these 12 eigenvalues between a very fast value which may become unstable with sampling and a very low value which may degrade closed loop bandwidth. (for instance, the joint configuration $Q = [8.5 \quad -5.8 \quad -23.3 \quad 13.0 \quad 36.3 \quad 25.1]^T(mm)$ with $\omega = 30rd/s$ leads to :$0.23 < \Re(\lambda_i) < 11700 \quad rd/s$!!).
- in the second case, this spreading out is significantly reduced ($10. < \Re(\lambda_i) < 50. \quad rd/s$ in the same conditions) and so expresses that dynamic behavior is governed by rotor inertias whose amplification by transmission ratio square freezes the joint dynamic models for any configuration.

So, paradoxically, we will choose a tuning based on the joint dynamic model to control this particular parallel concept. From the proximity information δX and joint rate measurements $\dot{Q}_m$, this control reads:

$$U = A_0 \left[J^{-1}(Q).K_p.\delta X - K_v \dot{Q}_m \right]$$

Note: From implantation point of view, this control requires only inverse Jacobian computation which is straight.

3.4 Connection to the macro-manipulator

The control schema proposed below (figure 4) is derived from position-force hybrid control architecture developed in [6] for an active parallel wrist mounted on a serial manipulator (SCARA). The proximity information availability and the absence of force control requirement allow to simplify the schema: the proximity measurement (δX_m) is sent straightforwardly to the dexterous manipulator controlled by the previous law while the macro manipulator is servo-looped onto the Cartesian position of the end effector (AB_m) (computed via the geometric model) which is then compared to the one obtained if the parallel manipulator stays in the middle configuration (AB_0).

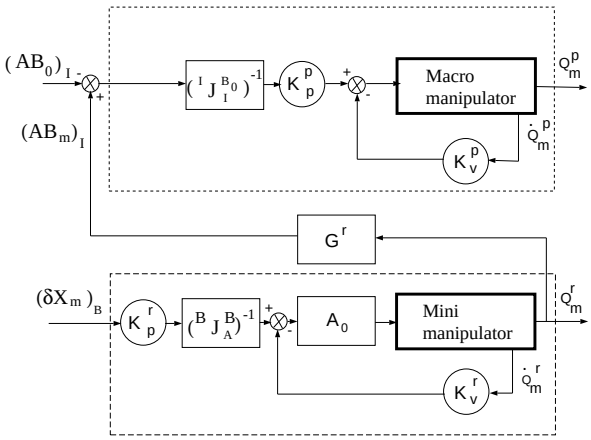

Figure 4 Coordinated control design

By this way, the end effector can follow target motion which presents high magnitudes at low frequencies and low magnitudes at high frequencies. The dexterous manipulator ability to reject perturbation due to macro manipulator motion depends upon their respective bandwidths and can be illustrated on the mono-dimensional equivalent case:

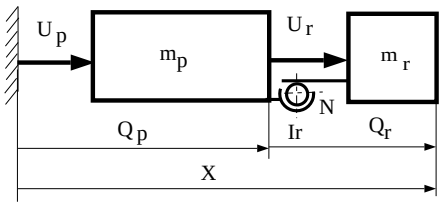

Figure 5 Equivalent mono-dimensional model

where indexes p and r are relative respectively to the macro and mini manipulator parameters. The open loop model is then reduced to:

$$\begin{bmatrix} m_p & m_r \\ m_r & m_r + I_r N^2 \end{bmatrix} \begin{bmatrix} \ddot{Q}_p \\ \ddot{Q}_r \end{bmatrix} = \begin{bmatrix} U_p \\ U_r \end{bmatrix};$$
$$X = Q_p + Q_r$$

and coordinate control simply reads:

$$U_p = K_p^p Q_r - K_v^p \dot{Q}_p$$
$$U_r = K_p^r \delta X - K_v^r \dot{Q}_r \ ; \ with \ \ \delta X = X_{ref} - X$$

It is easy to show that closed loop transfer function reads:

$$\frac{X}{X_{ref}}(s) = \frac{\Psi_p(s)}{\Psi_p(s)\Psi_r(s) + \varepsilon(s)} \ ; \ \text{where :}$$

- $\Psi_p(s) = \frac{m_p}{K_p^p}s^2 + \frac{K_v^p}{K_p^p}s + 1$ represents the characteristic polynomial of the macro-manipulator (low dynamic),
- $\Psi_r(s) = \frac{m_r + I_r N^2}{K_p^r}s^2 + \frac{K_v^r}{K_p^r}s + 1$ represents the characteristic polynomial of the mini-manipulator (high dynamic),
- $\varepsilon(s) = \frac{m_r I_r N^2}{K_p^p K_p^r}s^4 + \frac{m_r K_v^r}{K_p^p K_p^r}s^3 - \frac{I_r N^2}{K_p^r}s^2 - \frac{K_v^p}{K_p^r}s$ represents the residue (macro-manipulator mass independent) which expresses that the low dynamic, seen from the end effector position, is not completely unobservable.

We have shown in [2] that:

- this residue is all the more negligible since the mass ratio m_r/m_p between the mini and the macro-manipulator is low and since the tuning pulsation ratio ω_p/ω_r between the macro and the mini manipulator is also low (assuming an over-damped tuning for both manipulator: $K_p^i = m_i.\omega_i^2$ et $K_v^i = 2.m_i.\omega_i$ with $i = r$ or p),
- the rotor apparent mass has not significant influence on the closed loop dynamic and on the residue,
- this residue vanishes totally if we consider the following coordinate control, which assumes at our disposal the end effector Cartesian rate measurement:

$$U_p = K_p^p Q_r - K_v^p \dot{Q}_p$$
$$U_r = K_p^r \delta X - K_v^r \dot{\delta X}$$

In our application, we can check that the equivalent mono-dimensional mass ratio in each Cartesian direction is always very low and the tuning of the control laws presented in previous sections ($\omega_p = 4rd/s$ and $\omega_r = 30rd/s$) leads to an suitable pulsation ratio.

3.5 Simulation results

Simulation of the two manipulators set has been led with SDFAST software and required to take into account 26 bodies: 1 for the carrier vehicle, 6 for the macro-manipulator and 19 for the parallel manipulator (the lower plate is now attached to the macro manipulator last body). We want to highlight 2 points:

- for the study of the parallel manipulator cantilevered on a fixe base, it is possible to omit the six rotor bodies by increasing the jack piston masses with the corresponding apparent masses. The dynamic model stays quite representative, but it is no longer possible when this manipulator is mounted on a moving base because the inertial forces applied on this base by the mini-manipulator would no longer be realistic,
- by comparison with the two other solutions we have to note that macro-manipulator rotor modes are not taken into account (in order to decrease the number of bodies). But this imperfection is not determinant in the parallel case because the coordinate control does not require high dynamic performances for the macro-manipulator (condition on pulsation ratio).

The time response of the end effector along the nominal motion is displayed on figure 10. The tracking error is negligible for any Cartesian direction. It can be shown [2] that the jack extensions stay under 5 cm on this 30 cm along Ax axis deployment. That gives an idea of the macro-manipulator contribution to increase the mini-manipulator work-space without performance degradations.

Conclusions

This analysis, led around the three solutions:

- macro-manipulator with closed loop Cartesian control by the means of a proximity sensor,
- serial mini-manipulator concept and
- parallel mini-manipulator concept,

now enables us to conclude that a dexterous manipulator is essential to reach a closed loop bandwidth, able to reject dynamic perturbations (mainly dry friction) and to achieve tracking error under 1 mm. In the first case the bandwidth is limited by in-joint rotor mode (4rd/s). In the second case, this is again the flexibility of the structure composed of the macro-manipulator in parallel with the anchorage device which limits the closed loop dynamic (20 rd/s) by the fact of the non-collocation between the measurement (proximity sensor) and the control torques. Significant improvements can be done by creating artificial damping with the macro manipulator joints whose stiffness are redundant with the anchorage system. The best results have been carried out with the parallel concept (30 rd/s) but this concept involves a coordinate control between the 12 d.o.f. of the set of both manipulators.

References

[1] D. Alazard and J.P. Chrétien. Flexible joint control: robustness analysis of the collocated and non-collocated feedbacks. In *IROS, Intelligent RObot Systems*, Yokohama.Japan, July 26-30 1993.

[2] D. Alazard D. and J. P. Chrétien. Commande coordonnée d'un Organe Terminal Dextre (OTD) porté par un manipulateur externe: Comparaison des performances des concepts séri et parallèle. Rapport Final 2/7851a(texte), b(planches), CNES/DERA, Juin 1993.

[3] J. P. Chrétien. Documentation du logiciel smasp. Rapport Technique 2/7448, MATRA/DERA, 1985.

[4] C. Reboulet and T. Berthomieu. Dynamic models of six d.o.f. parallel manipulators. In *ICAR*, Pise.Italia, June 1991.

[5] D. Alazard D. and J. P. Chrétien. Commande coordonnée d'un Organe Terminal Dextre (OTD) porté par un manipulateur externe: Modélisation et commande des repositionneurs. Rapport Final 2/7813a(texte), b(planches), CNES/DERA, Septembre 1992.

[6] T. Berthomieu. *Etude d'un micro manipulateur parallèle et de son couplage avec un robot porteur*. Ph.d., Ecole Nationale Superieure de l' Aéronautique et de l'Espace, Janvier 1990. 1989.

[7] C. Reboulet. Commande des robots manipulateur. Note de cours, Ecole Natinonale Superieure de l' Aéronautique et de l'Espace, 1993.

[8] E.F. Fichter. A stewart platform-based manipulator: General theory and practical construction. In *The Interbnational Journal of Robotics Research*, volume Vol.5,N.2, 1986.

Figure 6 Macro-manipulator configuration (Continued) . . .

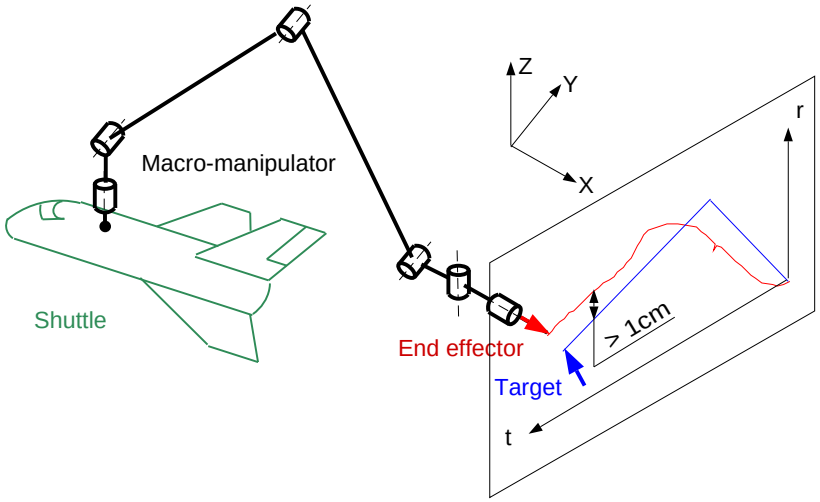

Figure 6 Macro-manipulator configuration

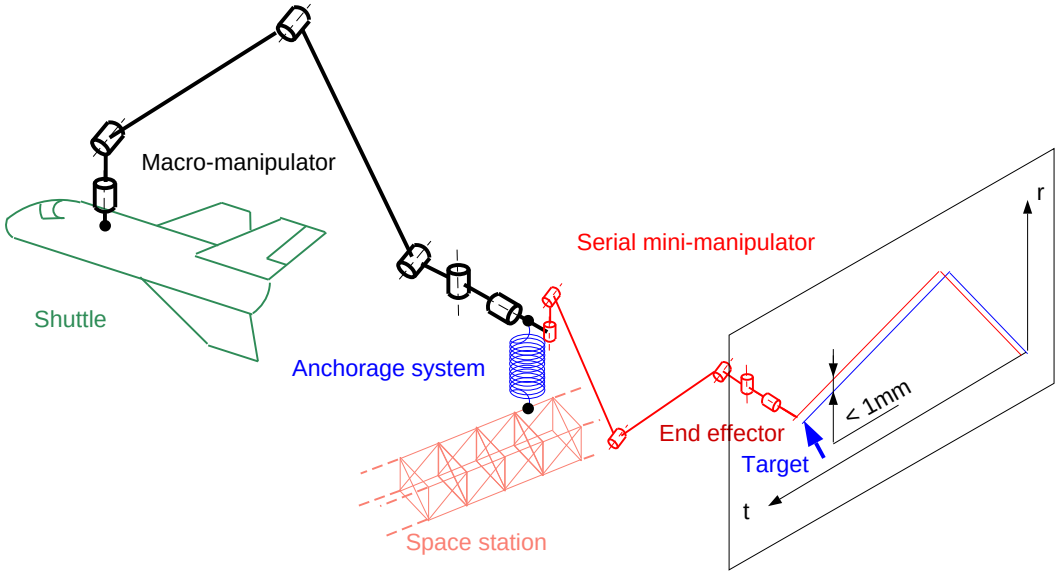

Figure 7 Serial mini-manipulator configuration (static positioning)

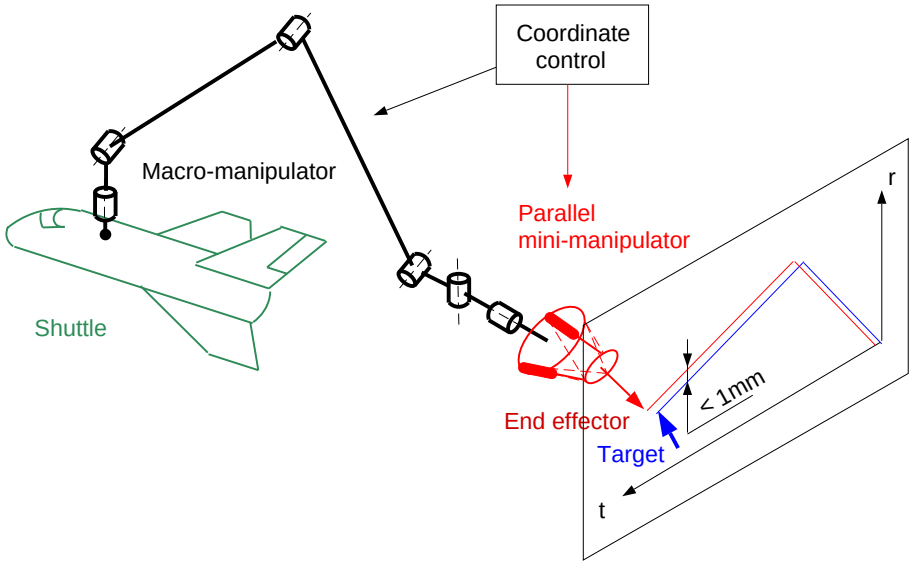

Figure 8 Parallel mini-manipulator configuration (dynamic positioning)

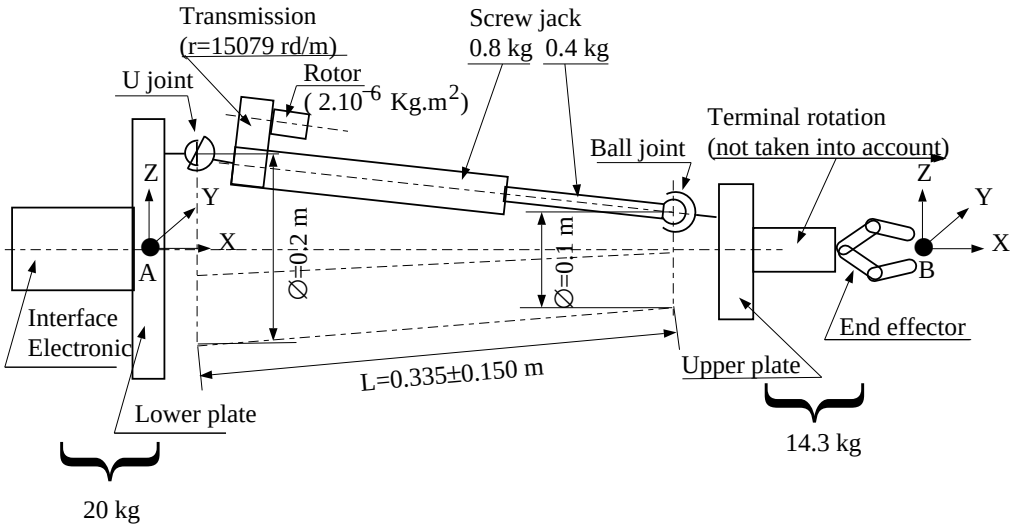

Figure 9 Parallel manipulator (middle configuration)

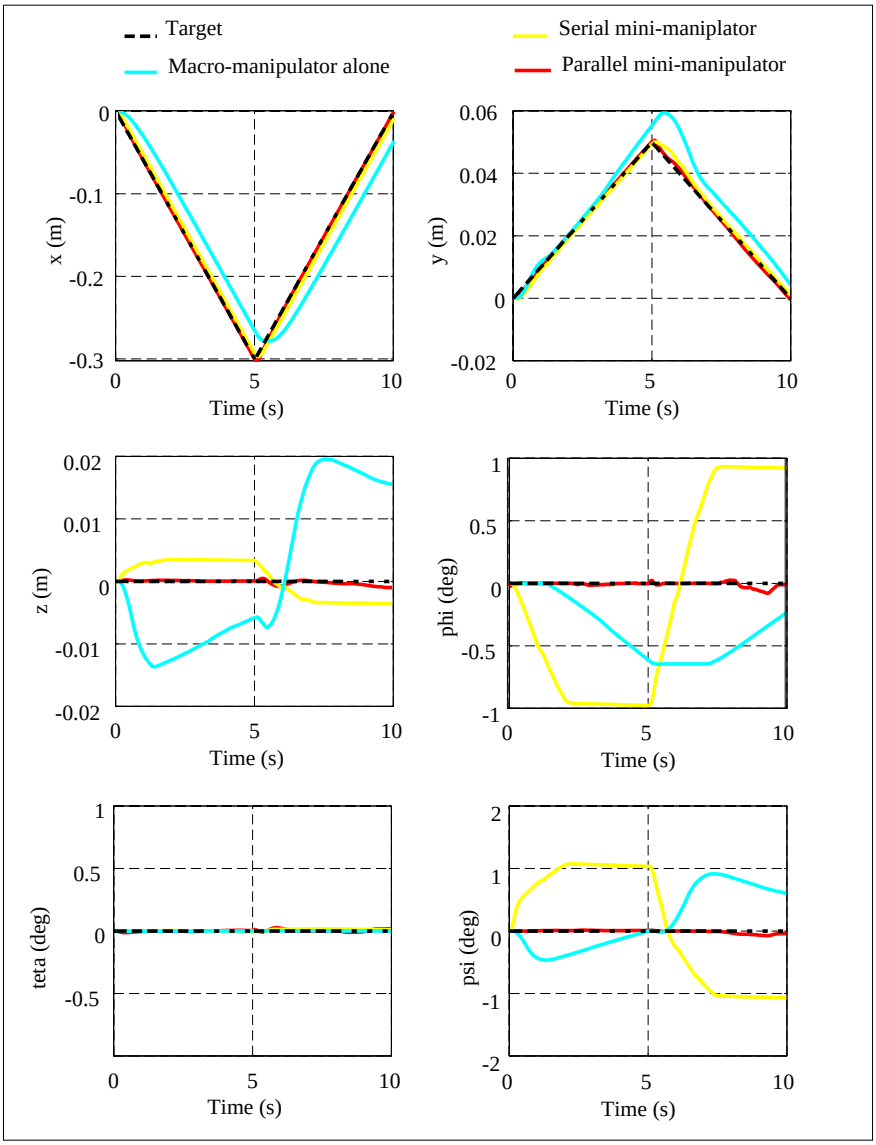

Figure 10 Comparative simulation results